Pattern Formation at the Traveling Liquid-Crystal Twist-Grain-Boundary–Smectic-A Interface

P. E. Cladis,[1] A. J. Slaney,[2] John W. Goodby,[2] and Helmut R. Brand[3]

[1]*AT&T Bell Laboratories, Murray Hill, New Jersey 07974*
[2]*School of Chemistry, University of Hull, Hull HU6 7RX, United Kingdom*
[3]*Theoretische Physik III, Universität Bayreuth, D95440 Bayreuth, Federal Republic of Germany*
(Received 30 August 1993)

The different patterns observed at a twist-grain-boundary– (TGB$_A$–) smectic-A (A) interface moving in a temperature gradient are quantified by measuring interface arclength scaling between two lengths characterizing these patterns. The ragged melting TGB$_A$-A interface results from the growth of TGB$_A$ filaments into oriented A. We attribute the destruction of TGB$_A$ when A grows into TGB$_A$ to the second-order nature of the TGB$_A$-cholesteric transition. These results are interpreted within a defect lattice model.

Pattern formation at phase boundaries moving in a temperature gradient is a major area of nonequilibrium physics attracting considerable attention [1]. While most of the early work concentrated on moving solid-liquid interfaces, now the focus has changed to phase transitions characterized by broken continuous symmetries [1]. Most recently, we investigated consequences to interfacial patterns of a chirality-induced equilibrium length [2].

Here, we study pattern formation at another chiral interface where one of the phases has a chirality-induced defect lattice, the twist-grain-boundary (TGB) phase. The TGB state is analogous to the vortex lattice in type II superconductors predicted by de Gennes' analogy between the nematic–smectic-A (N-A) transition and the normal-superconducting transition [3]. Nematic and smectic-A liquid crystals are anisotropic systems with long range orientational order along a director $\hat{n}$. Smectic A is also layered with $\hat{n}\|$ to the layer normals. Close to a weakly first-order N-A transition, layer fluctuations are large [4] and anisotropic being larger $\|\hat{n}$ than $\perp\hat{n}$ [5] so that κ the Ginzburg parameter [3] distinguishing between type I ($\kappa < 1/\sqrt{2}$) and type II ($\kappa > 1/\sqrt{2}$) behavior is such that $\kappa_\| < \kappa_\perp$. Loosely speaking, TGB phases are more similar to the vortex lattice of anisotropic ceramic [6] than of metallic superconductors.

Cholesterics (N^*), which show broken rotational symmetry as nematics, have, in addition, a helix structure with curl$\hat{n} \perp \hat{n}$. In de Gennes' model, curl$\hat{n}$ is analogous to an applied field $\mathbf{H} =$curl$\mathbf{A}$, where $\mathbf{A}$ is the vector potential: The cholesteric–smectic-A transition is necessarily first order [7]. Consequently, Renn and Lubensky [8] investigated the superconducting–smectic-A analogy for a first-order N^*-A transition. They found that type II behavior could be exhibited at this transition provided layer fluctuations $\perp\hat{n}$ were small and the helix pitch ($2\pi/q_0$) at the N^*-A transition large enough.

Independently, Goodby et al. [9] observed an unusual state between the isotropic liquid and the smectic-C^* phase, layered like smectic A but with $\hat{n}$ inclined to the layer normal and a helix structure. As x-ray diffraction showed this novel state to be layered, they concluded they

had observed the first TGB phase and confirmed its dislocation structure with freeze fracture observations [9]. While more investigations [9–11] of this novel state followed, up to now all physical investigations have been at a TGB phase above smectic C^*.

Here we report the first dynamic experiments on a pure compound showing a TGB phase between a smectic-A and a cholesteric phase [12]. The TGB$_A$-A phase boundary is well defined and exhibits different patterns depending on whether TGB$_A$ grows or smectic A grows. TGB$_A$ only grows into well-oriented A. As it cannot propagate into N^*, it is eventually squeezed out as N^* A grows, leaving behind a direct N^*-A phase boundary. We quantify differences in these patterns by measuring their arclengths and positions in the temperature gradient as a function of interface velocity and interpret these results in the context of the Renn-Lubensky model [8] and a constrained type II N^*-A transition.

The material is 12O2Cl4M5T [(S)-2-chloro-4-methylpentyl 4'-(4-n-dodecyloxypropioloyloxy)-4-biphenylcarboxylate] [12] and its phase sequence was determined by differential scanning calorimetry and observations of its textures in the polarizing microscope. While in calorimetry, the heat of transition for the TGB$_A$-A transition is too small to measure (TGB$_A$ refers to TGB phases containing blocks of smectic A [8]); its onset at 107.5 °C is observed in the polarizing microscope as a bright wavy filamentary texture [Fig. 1(a)] against a uniform homeotropic (optic axis, $\hat{n}$, $\|$ viewing direction) smectic-A background. In contrast, the TGB$_A$-N^* transition at 111 °C has a measurable heat of transition (~ 0.1 cal/g) but its phase boundary is not observed in the polarizing microscope.

Figure 1(a) (top) shows a nearly periodic filamentary texture exhibited by TGB$_A$ as it nucleates and grows from the edges of a 50 μm flat capillary at constant temperature into oriented A. The wavelength of this texture is $\lambda_0 = 3.5$ μm. Slightly raising the temperature results in the filaments nonuniformly lengthening and even bending as they grow. However, while the average distance between filaments changes as they lengthen, their width
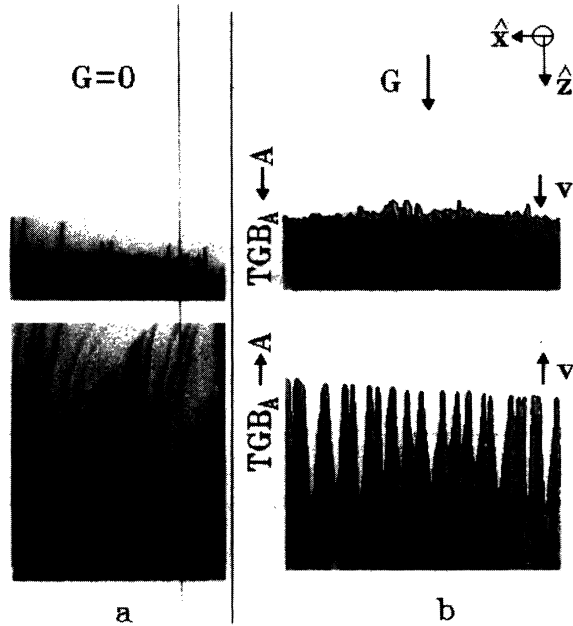
FIG. 1. (a) TGB$_A$'s filamentary growth habit into oriented smectic A at fixed temperature. The wavelength in the top picture is $\lambda_0 = 3.5$ μm and the temperature is close to the TGB$_A$-A transition temperature, i.e., $\approx 107.5\,°$C. In the bottom pattern, the temperature is slightly higher (about $108\,°$C): While the filaments are longer, they are the same width as in the top picture. (b) The freezing (top) and melting (bottom) patterns at the traveling TGB$_A$ interface in a temperature gradient G. The interface velocity is shown for $A \rightarrow$ TGB$_A$ (TGB$_A$ melting) and TGB$_A \rightarrow A$ (TGB$_A$ growing). The coordinate system used here is at the top of (b) with the positive y axis pointing into the plane of the figure. The magnification in (b) is half that of (a).

does not [bottom, Fig. 1(a)].

In a constant temperature gradient, G, the moving TGB$_A$-A interface shows patterns both on "freezing" [Fig. 1(b), top, moving the sample towards the cold contact, so $A \rightarrow$ TGB$_A$] as well as on "melting" [Fig. 1(b), bottom, moving the sample towards the hot contact, so TGB$_A \rightarrow A$]. The same filaments as shown in Fig. 1(a) are the smallest coherent structure in the patterns when boundary conditions for A are well defined as they are in Fig. 1. The fixed width of the growth filaments parallel to the interface and the broadband of their length scales perpendicular to it [Fig. 1(a)] are responsible for the unusual observation of a ragged interface for the melting TGB$_A \rightarrow A$ interface [Fig. 1(b)]. Impurity diffusion is too fast to account for the ragged TGB$_A \rightarrow A$ interface on the time scales of these experiments (hours).

The sample is contained in a flat glass capillary of the following dimensions: thickness $h = 50$ μm ($\parallel$ to the viewing direction $\hat{y}$); width $w = 1$ mm ($\parallel \hat{x}$); and length $L = 50$ mm ($\parallel$G$\parallel \hat{z}$). Its interior has been prepared such that the director at the surface is $\hat{n} \parallel \hat{y}$. The sample is transported at constant speed (*pulling speed* v) through a temperature gradient $|$G$| = 2.2$ K/mm. The moving TGB$_A$-A interface is observed far from the sidewalls at
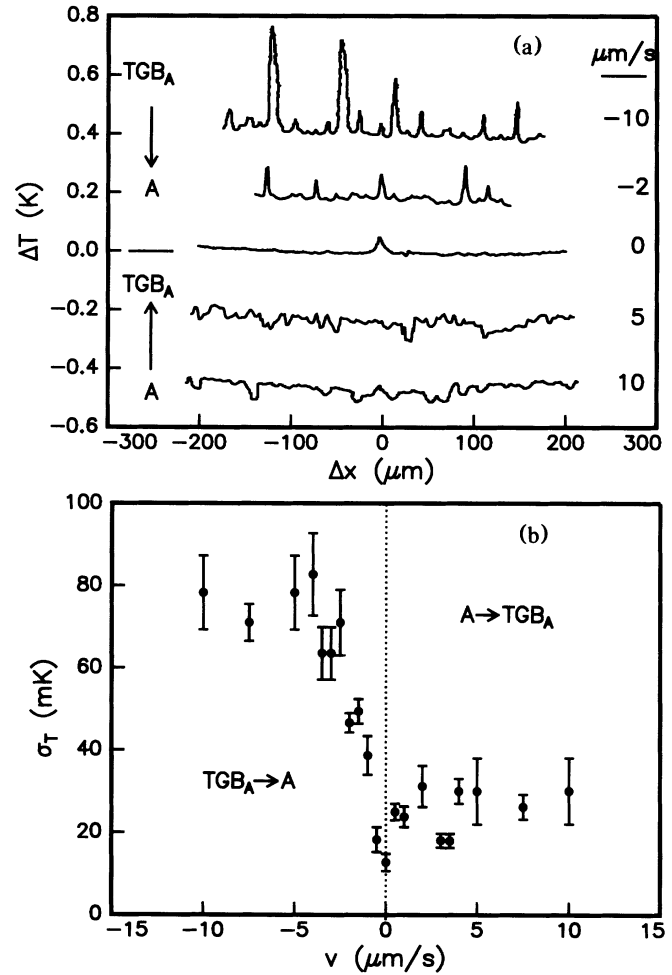

FIG. 2. (a) Data obtained by digitizing the TGB$_A$ interfaces using a left-hand walker algorithm [14] are shown as a function of space (x) and their position in the temperature gradient relative to the rest position for different pulling speeds. The left-hand walker moves 1 pixel per step along the interface. (b) The pattern amplitude measured by the standard deviation from their mean position vs v.

$x = 0$ and $x = w$ with a polarizing microscope and an image analysis system [13].

In these experiments, temperature is mapped onto the spatial dimension z. Figure 2(a) shows typical length and temperature scales of the patterns and their observed positions in the temperature gradient. Figure 2(b) shows the pattern amplitudes, ΔT, in degrees kelvin, K, measured by their standard deviation, σ_T, from their respective mean positions. Figures 2 show both qualitative and quantitative differences between patterns where TGB$_A \rightarrow A$ and $A \rightarrow$ TGB$_A$: Freezing patterns have a smaller amplitude and wavelength compared to melting patterns.

We estimate the Ginzburg parameter for twist [8] κ_2 by assuming that at a first-order A-TGB$_A$ transition, the free energy density of a cholesteric is not very different from that of TGB$_A$. Then, $\kappa_2 = (d/2\pi)/\sqrt{2}q_0\xi_c^2$, where

$d \approx 40$ Å is the smectic-A layer spacing, $2\pi/q_0$ is the helix pitch at T_c, and ξ_c is the coherence length at T_c for layer fluctuations $\perp \hat{n}$. From measured maximum ($\Delta T_{max} \approx +0.5$ K) and minimum ($\Delta T_{min} \approx -0.5$ K) temperature differences of the interface with pulling speed, we deduce $\epsilon_c \equiv |T^* - T_c|/T_c = \Delta T_{max}/T_c \approx 1.5 \times 10^{-3}$. Taking ξ_0 as the molecular diameter, 5 Å [4], $\xi_c = \xi_0/\sqrt{\epsilon_c} \approx 140$ Å. The pitch at T_c is taken to be the filament width that first appears at TGB$_A \rightarrow A$ [Fig. 1(a)], $q_0 = 2\pi/\lambda_0$. With these assumptions, we find $\kappa_2 \approx 3/\sqrt{2}$: While the blocks of smectic A separated by screw dislocation walls are only $\xi_c \approx 140$ Å wide and so not distinguishable from a cholesteric with a uniform twist in the polarizing microscope, this N^*-A transition must be interpreted in a type II context.

Where classical methods, e.g., power spectra and self-affine fractals, fail to quantitatively distinguish between melting and freezing patterns [Figs. 1(b) and 2], analysis of their arclengths (S) [15] as a function of the number of steps (n) to cover the interface succeeds [Fig. 3(a)]. Patterns at this TGB$_A$ interface show scaling behavior [15] between two cutoff lengths: a longer one (≈ 28 μm) determined by sample thickness and a shorter one, by the filament width $\lambda_0 \approx 3.5$ μm [Fig. 1(a)].

To find the scaling relation between cutoffs, we put $S = A/n^{D-1} + B$, then determine A and B from the conditions $S = S_{max}$ when $n = n_{max} \rightarrow \infty$ and $S = S_0$ (the flat interface) when $n = n_c$. We fit the data [see, e.g., Fig. 3(a)] to

$$\frac{1 - S/S_{max}}{1 - S_0/S_{max}} = \left[\frac{n_c}{n} \right]^{D-1}. \tag{1}$$

S_{max} is defined as the arclength obtained at the resolution of 1 pixel (0.9 μm) and S_0 is the distance between the first and last points on the interface in the field of view. From these fits, we obtain n_c and hence a cutoff length λ_c from the step size corresponding to it. We also obtain the exponent D. About 100 interfacial patterns with file size ranging from ≈ 1000 to 3500 points have been analyzed as a function of interface speed v. The range of fits was about one decade for $A \rightarrow$ TGB$_A$, and about two decades for TGB$_A \rightarrow A$.

On the basis of this analysis and evident in Fig. 4, the patterns fall into three regimes [16]:

(1) A small amplitude ($\sigma_T \approx 25$ mK corresponding to a length of 11.4 μm for $G = 2.2$ K/mm [Fig. 2(b)]) *freezing regime* limited by λ_0 and sample thickness. Its long wavelength cutoff, nearly independent of pulling speed, is $\langle \lambda_c \rangle_F = 11.8 \pm 1.2$ μm $\approx \sqrt{\lambda_0 h/2}$. The steady state temperature shift of the interface depends linearly on speed, reaching ≈ -0.5 K when $v = 10$ μm/s [Fig. 2(a)]. In this regime, TGB$_A$ disappears in $\approx 3 \times 10^3$ s at $v = 1$ μm/s and in $\approx 6 \times 10^2$ s at 10 μm/s.

(2) A *transition regime* between rest and $v \approx -2$ μm/s where $\langle \lambda_c \rangle$ grows from ≈ 11.8 μm to $\langle \lambda_c \rangle_M \approx 2\langle \lambda_c \rangle_F$. In this regime, the interface moves to succes-
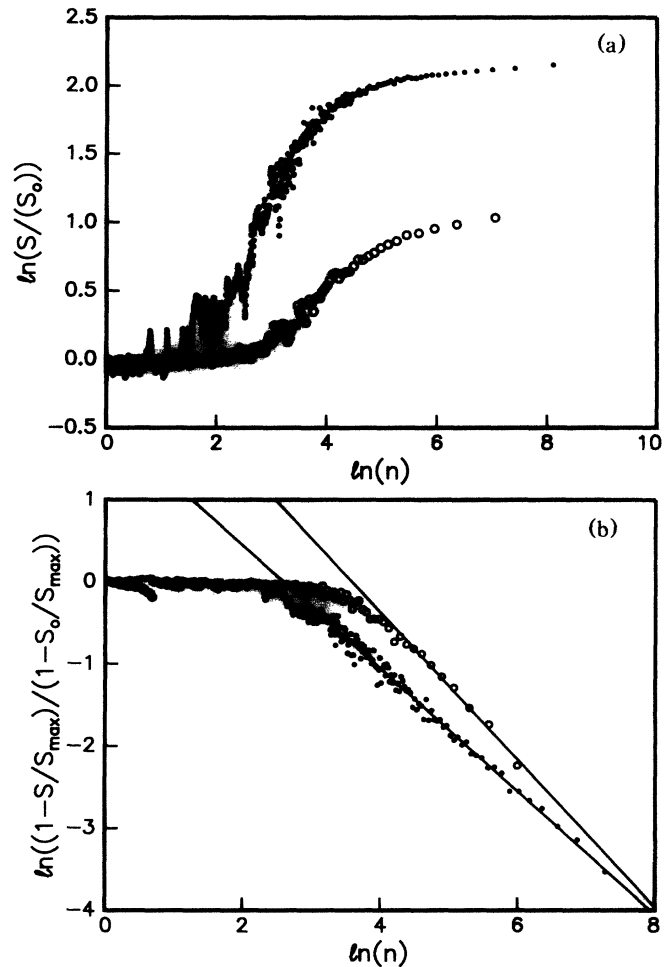

FIG. 3. (a) The interfacial arclength S scaled by the flat interface length S_0 vs the number of steps n to cover the interface (Fig. 2). The larger step cutoff (smaller n) is related to sample thickness and the smaller cutoff (larger n) is λ_0 [Fig. 1(a)]. (b) Fit of the scaling regime for data such as shown in (a): ●, TGB$_A \rightarrow A$; ○, $A \rightarrow$ TGB$_A$. Here, $v = |5 \mu$m/s$|$.

sively warmer average positions in the gradient as the absolute pulling speed increases from rest to 2 μm/s reaching a maximum shift, ≈ 0.5 K, when $|v| > 2.5$ μm/s.

(3) A large amplitude ($\sigma_T \sim 73$ mK $\leftrightarrow 33$ μm) *melting regime* for $v < -2$ μm/s, where $\langle \lambda_c \rangle_M \approx 26.8 \pm 1.8$ μm and $D = 1.73 \pm 0.02$ are nearly independent of v. In this regime, TGB$_A$ grows.

The short wavelength cutoff is deduced from data [e.g., Fig. 3(a)] and found to be $\approx \lambda_0$, the filament width at T_c [Fig. 1(a)]. Both freezing and melting patterns have a long wavelength cutoff, λ_c, where for step sizes greater than λ_c the interface is flat ($D = 1$): Sample thickness introduces a gap in the band of wave numbers, k, in the pattern: as $k \rightarrow 2\pi/\lambda_0$ (i.e., the q_0 used to estimate κ_2) arclength scales between λ_c and λ_0 with exponent $D = 1.7$ reminiscent of 2D diffusion limited aggregation patterns for TGB$_A \rightarrow A$ and $D = 1.9$ for $A \rightarrow$ TGB$_A$, a more disordered pattern.
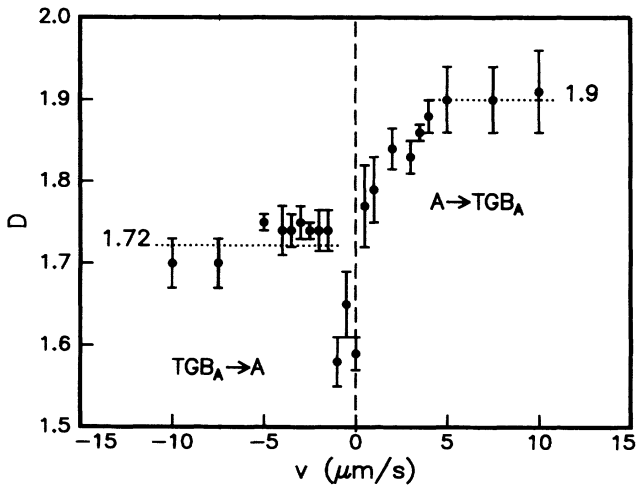
FIG. 4. The scaling exponent D vs interface velocity v determined from, e.g., Fig. 3(b) has three regimes.

What needs to be explained is why the short wavelength cutoff is much larger than ξ_c, the Renn-Lubensky [8] length for TGB_A. We suggest that this result can be traced back to the boundary conditions determined by sample preparation that constrain the A phase such that $\hat{n} \parallel \hat{y}$. Then, the smallest unit of TGB_A that can grow into the oriented A phase are the filaments [Fig. 1(a)] with a quantized amount of twist satisfying these boundary conditions. Given the small size of ξ_c, cholesteric and TGB_A are not distinguishable in an optical microscope; however, they are distinguishable by their different growth dynamics into an oriented A phase: The melting cholesteric-A interface is flat [17] while the TGB_A-A interface is ragged. Thus, we attribute both short and long wavelength cutoffs in the patterns to sample preparations constraining $\hat{n} \parallel \hat{y}$ in the A phase.

The well-defined TGB_A-A boundary is consistent with a weakly first-order TGB_A-A transition and the poorly defined TGB_A-cholesteric phase boundary with a mean-field second-order TGB_A-cholesteric transition [8] at which TGB_A cannot propagate into the cholesteric phase [18]. Thus, $A \rightarrow TGB_A$ until it reaches the immobile TGB_A-cholesteric phase boundary. As A grows, it expels curl$\hat{n}$ into TGB_A driving $\kappa_2 \rightarrow 1/\sqrt{2}$, i.e., eventually squeezing out TGB_A, leaving behind a disordered, direct smectic-$A \rightarrow$ cholesteric phase boundary.

To summarize, depending on whether $A \rightarrow TGB_A$ or $TGB_A \rightarrow A$, qualitatively different patterns are observed. Indeed, this may be the first time a steady state pattern is observed in directional melting. When they are not simply periodic, directional growth patterns are difficult to characterize physically [1]. The novelty of our analysis is that arclengths of the traveling phase boundaries are used to obtain quantitative information. Two lengths emerged from this analysis: a longer one set by sample thickness and a shorter one associated with the smallest unit of

TGB_A that can grow into an oriented A phase. Being a first-order transition, the A-TGB_A phase boundary can propagate either way. A second-order TGB_A-cholesteric transition [8] is consistent with observations that this phase boundary is visually poorly defined and does not propagate into the cholesteric state: As smectic A grows, TGB_A is eventually squeezed out, leaving behind a direct smectic-$A \rightarrow$ cholesteric phase boundary.

[1] See, for example, Propagation in Systems Far from Equilibrium, edited by J. E. Wesfreid et al. (Springer, New York, 1988); J. M. Flesselles, A. J. Simon, and A. J. Libchaber, Adv. Phys. 40, 1 (1991); Pattern Formation in Complex Dissipative Systems, edited by S. Kai (World Scientific, Singapore, 1992); M. C. Cross and P. C. Hohenberg, Rev. Mod. Phys. 65, 851 (1993).

[2] P. E. Cladis, J. T. Gleeson, P. L. Finn, and H. R. Brand, Phys. Rev. Lett. 67, 3239 (1991).

[3] P. G. de Gennes, Solid State Commun. 10, 753 (1972).

[4] B. I. Halperin and T. C. Lubensky, Solid State Commun. 14, 997 (1974).

[5] B. M. Ocko, R. J. Birgeneau, and J. D. Litster, Z. Phys. B 62, 487 (1986); B. R. Patton and B. S. Andereck, Phys. Rev. Lett. 69, 1556 (1992).

[6] G. Blatter, M. V. Feigel'man, V. B. Geshkenbein, A. I. Larkin, and V. M. Vinokur, "Vortices in High Temperature Superconductors" (to be published).

[7] T. Lubensky, J. Phys. (Paris), Colloq. 36, C1-151 (1975); P. B. Vigman and V. M. Filev, Zh. Eksp. Teor. Fiz. 69, 1466 (1975) [Sov. Phys. JETP 42, 747 (1975)].

[8] S. R. Renn and T. C. Lubensky, Phys. Rev. A 38, 2132 (1988).

[9] J. W. Goodby, M. A. Waugh, S. M. Stein, E. Chin, R. Pindak, and J. S. Patel, J. Am. Chem. Soc. 111, 8119 (1989); K. J. Ihn, J. A. N. Zasadzinski, R. Pindak, A. J. Slaney, and J. W. Goodby, Science 258, 275 (1992); G. Srajer, R. Pindak, M. A. Waugh, J. W. Goodby, and J. S. Patel, Phys. Rev. Lett. 64, 1545 (1990).

[10] L. Navailles, P. Barois, and H. T. Nguyen, Phys. Rev. Lett. 71, 545 (1993).

[11] S. R. Renn, Phys. Rev. A 45, 953 (1992).

[12] A. J. Slaney, Ph.D. thesis, University of Hull, 1992 (unpublished).

[13] See, for example, P. E. Cladis, J. T. Gleeson, and P.L. Finn, Phys. Rev. A 44, R6173 (1991), and references therein.

[14] J. T. Gleeson, Ph.D. thesis, Kent State University, 1992 (unpublished).

[15] B. B. Mandelbrot, Fractal Geometry of Nature (Freeman, San Francisco, 1982).

[16] P. E. Cladis et al. (to be published).

[17] P. Oswald, J. Bechhoefer, A. Libchaber, and F. Lequeux, Phys. Rev. A 36, 5832 (1987).

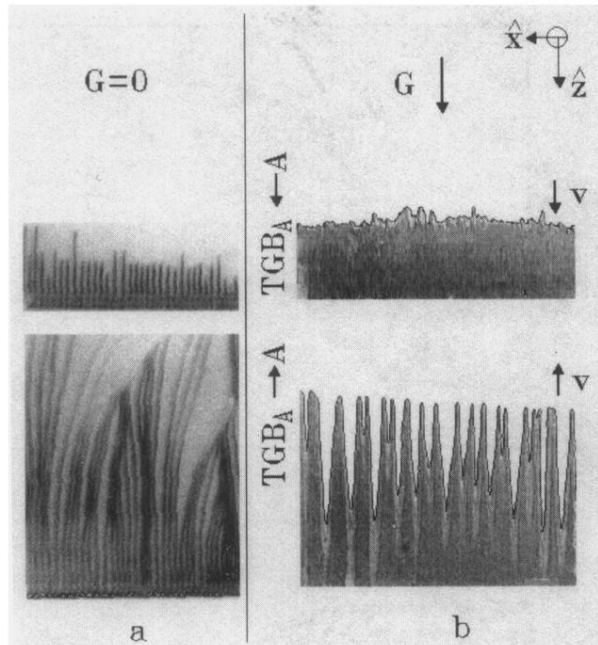[18] P. E. Cladis, J. Stat. Phys. 62, 899 (1991).

FIG. 1. (a) TGB$_A$'s filamentary growth habit into oriented smectic A at fixed temperature. The wavelength in the top picture is $\lambda_0 = 3.5$ μm and the temperature is close to the TGB$_A$-A transition temperature, i.e., $\approx 107.5\,°$C. In the bottom pattern, the temperature is slightly higher (about $108\,°$C): While the filaments are longer, they are the same width as in the top picture. (b) The freezing (top) and melting (bottom) patterns at the traveling TGB$_A$ interface in a temperature gradient **G**. The interface velocity is shown for $A \to$ TGB$_A$ (TGB$_A$ melting) and TGB$_A \to A$ (TGB$_A$ growing). The coordinate system used here is at the top of (b) with the positive y axis pointing into the plane of the figure. The magnification in (b) is half that of (a).